Nanoscale

PAPER



Cite this: *Nanoscale*, 2019, **11**, 15245

# Water-soluble chiral CdSe/CdS dot/rod nanocrystals for two-photon fluorescence lifetime imaging and photodynamic therapy†

Tingchao He,[a] Xin Qiu,[a] Junzi Li,[a] Guotao Pang,[b] Zizi Wu,[c] Jiaji Cheng,[a] Ziming Zhou,[b] Junjie Hao,[b] Haochen Liu,[b] Yun Ni,[c] Lin Li,[c] Xiaodong Lin,[a] Wenbo Hu,*[c] Kai Wang*[b] and Rui Chen*[b]

Received 27th May 2019,
Accepted 23rd July 2019

DOI: 10.1039/c9nr04508b

rsc.li/nanoscale

Compared with traditional organic contrast agents, semiconductor nanocrystals (NCs) have unique optical properties that are vital for biological applications with ultrahigh sensitivities, such as long fluorescence lifetime and large multiphoton absorption (MPA). However, the MPA properties and biological applications of chiral-ligand-stabilized semiconductor NCs have scarcely been reported, which seriously hinders their relevant applications. In this work, we report the aqueous phase transfer of CdSe/CdS dot/rod NCs with the use of cysteine molecules, after which the NCs preserve their high fluorescence quantum yield, long lifetime, and efficient circular dichroism. More importantly, the investigated dot/rod NCs show extremely large two- and three-photon absorption action cross-sections in the first and second biological windows, with maximum values of ~21 000 GM at 800 nm and ~4.6 × $10^{-78}$ $cm^6$ $s^2$ per photon$^2$ at 1300 nm, which are among the largest values reported for water-soluble fluorescent nanoparticles. Interestingly, the dot/rod NCs exhibit a high singlet oxygen generation efficiency of 35%. In addition, for the first time, two-photon fluorescence lifetime imaging and photodynamic therapy of the dot/rod NCs were successfully demonstrated. The performed investigation of the optical properties of these water-soluble CdSe/CdS dot/rod NCs indicates that they are promising candidates for nonlinear biological imaging applications.

## Introduction

In recent decades, semiconductor nanocrystals (NCs) have attracted substantial attention due to their wide use in numerous biological applications and optoelectronic devices.[1] Semiconductor NCs offer several advantages compared to organic dyes, including narrow emission spectrum, high brightness and stability against photobleaching.[2] Additionally, the development of semiconductor NCs with different morphologies, such as one-, two- and three-dimensional geometries, can introduce novel properties into the resulting systems.[3] For example, compared with their spherical counterparts, one-dimensional semiconductor nanorods usually exhibit much stronger multiphoton absorption (MPA) due to their enhanced quantum confinement effect. However, the existing literature reports only their MPA at select wavelengths.[4–7] To gain insight into the intrinsic features of semiconductor NCs, it is extremely important to characterize their MPA properties over a wide range of wavelengths to find the optimal excitation wavelengths for a given application.

Although the MPA properties of semiconductor NCs in organic solvents have been widely investigated, it is still a real challenge to achieve water-soluble semiconductor NCs with excellent photostability and efficient fluorescence emission for biological applications.[8–11] There are two approaches for the design of water-soluble NCs. The first method is based on a silica-coating approach,[12] while the other method involves organic coatings with linker molecules.[1] For example, Stasio *et al.* demonstrated that CdSe/CdS dot/rod NCs can be transferred into an aqueous environment by a ligand exchange method employing mercaptopropionic acid.[13] Among the

[a]*College of Physics and Optoelectronic Engineering, Shenzhen University, Shenzhen 518060, China*
[b]*Department of Electrical and Electronic Engineering, Southern University of Science and Technology, Shenzhen 518055, China. E-mail: wangk@sustech.edu.cn, chenr@sustech.edu.cn*
[c]*Key Laboratory of Flexible Electronics (KLOFE) & Institute of Advanced Materials (IAM), Jiangsu National Synergetic Innovation Center for Advanced Materials (SICAM), Nanjing Tech University (NanjingTech), Nanjing 211816, China. E-mail: iamwbhu@njtech.edu.cn*

†Electronic supplementary information (ESI) available: Experimental details of two-photon fluorescence lifetime imaging of living cells, measurements of the singlet oxygen generation ($^1O_2$) efficiency and two-photon photodynamic therapy. See DOI: 10.1039/c9nr04508b

various linker molecules, chiral ligands, such as cysteine, penicillamine and glutathione, have attracted increasing attention due to the possibility of imbuing chiroptical activity to the NCs that is induced by the chiral distortion of the surface atoms or orbital hybridization.[14–16] After surface functionalization with chiral molecules, the semiconductor NCs can be transferred to a nontoxic aqueous environment, which allows for their applications in bioimaging and chiral drug molecular recognition.[17] The combination of the decreased toxicity, chiral selectivity and large MPA of surface engineered semiconducting NCs can open new perspectives. Because chirality is an important phenomenon in living systems and nearly all biological fluorescent probes must be homochiral to function, the application of chiral CdSe/CdS dot/rod NCs will be especially important in various biological applications. However, to the best of our knowledge, the combination of MPA and chiroptical properties in a single NC and the relevant biological applications, including two-photon fluorescence lifetime imaging (FLIM) and photodynamic therapy (PDT), have never been reported, although it would represent a foundation for the development of novel nonlinear optoelectronic devices and biological applications.

Among the various semiconductor NCs, dot/rod NCs exhibit unique optoelectronic properties. On the one hand, dot/rod NCs have a quasi-1D electronic structure due to their small diameters; on the other hand, the quantum dot inside each nanorod exhibits 3D confinement and fully quantized states. For example, CdSe/CdS dot/rod nanoheterostructures in both organic and aqueous solutions were synthesized by several groups due to their luminescence with high quantum yield.[18,19] It was found that the dot/rod NCs exhibit interesting optical properties, including micro-lasers[20,21] and amazing MPA properties.[4–7] However, to date, only several studies on the MPA properties of dot/rod NCs in organic solvents have been reported.[4–7] It is therefore expected that both strong MPA properties and chirality can be combined in water-soluble CdSe/CdS dot/rod NCs capped with chiral ligands, which may be promising materials for various biological applications. Unfortunately, the development of such chiral dot/rod NCs remains a significant challenge, and no systematic studies of their MPA properties and relevant biological applications have been carried out to date. Thus, the relevant studies will provide insights into new biological applications of CdSe/CdS NCs associated with the chirality.

In this study, we synthesized two kinds of water-soluble cysteine-capped CdSe/CdS dot/rod NCs with different aspect ratios. The dot/rod NCs were found to exhibit high fluorescence quantum yields (QYs, $\eta$), efficient circular dichroism (CD) and ultrafast charge dynamic processes in the excited state. Importantly, the MPA cross-sections of the dot/rod NCs were also determined. More importantly, for the first time, we used the chiral structure of CdSe/CdS dot/rod heterostructures as highly efficient contrast agents to expand the applications of semiconductor NCs, including two-photon FLIM and PDT, which have never been revealed in previous literature studies.

## Results and discussion

### Steady-state spectroscopic properties of the CdSe/CdS dot/rod NCs

The morphology and size distribution of the CdSe/CdS dot/rod NCs were examined by transmission electron microscopy (TEM). The rod diameter was calculated to be ~4.6 nm, while the lengths were determined to be approximately 18 and 26 nm, respectively (Fig. 1a and b). The normalized linear absorption and photoluminescence (PL) spectra of the CdSe/CdS dot/rod NCs were measured (Fig. 1c). The dominant absorption band at higher energies is mainly associated with the lower transition in the CdS shell, while the small absorption peak at lower energies is attributed to the effective band edge transition in the CdSe core. The one-photon excited PL spectra of the dot/rod NCs with different lengths exhibit an average Stokes shift of ~10 nm, while the QYs of 18 and 26 nm long NCs were determined to be 3.2% and 3.3%, respectively. It should be noted that the PL peaks, *i.e.*, the peaks at 617 and 620 nm for the 18 and 26 nm long NCs, respectively, do not differ greatly between the different rod lengths due to the exponential decay rate of the CdSe electron wavefunction leaking into the CdS shell.[7] Thus, no significant redshifts are expected beyond a certain rod length. The PL lifetime values of the dot/rod NCs were then determined (Fig. 1d). These decay curves for the samples can be well fit to a biexponential decay function, giving averaged lifetime values of 8.5 and 11.4 ns for the 18 and 26 nm long rods, respectively. Compared to the 18 nm long rod, the 26 nm long rod exhibits a longer PL lifetime due to the electron–hole wavefunction overlap decreasing with increasing rod length.[7] The long CdSe/CdS dot/rod NC lifetime values enable them to be promising materials for FLIM.

The CD spectra of D- and L-cysteine-functionalized CdSe/CdS dot/rod NCs were then measured, and a mirrored CD line shape was observed for both the 18 and 26 nm long NCs

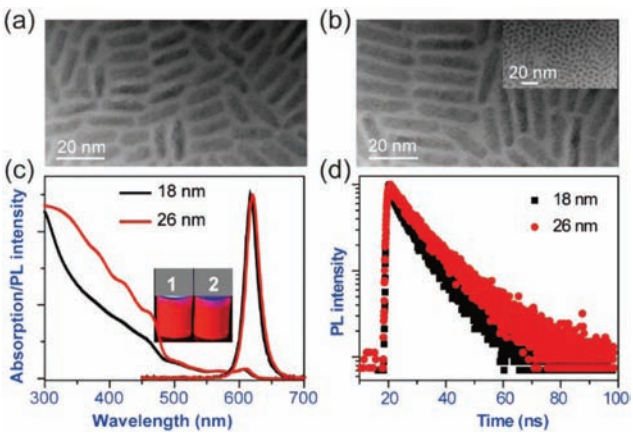


Fig. 1 (a and b) TEM images of the 18 and 26 nm long CdSe/CdS dot/rod NCs, respectively (white scale bar = 20 nm). The inset of (b) is the TEM image of the CdSe core. (c) The normalized absorption and one-photon excited PL spectra of the NCs. The insets are the emission images of the NCs in solution: 1 and 2 are the 18 and 26 nm long NCs, respectively. (d) PL decay curves for the 18 and 26 nm long NCs.

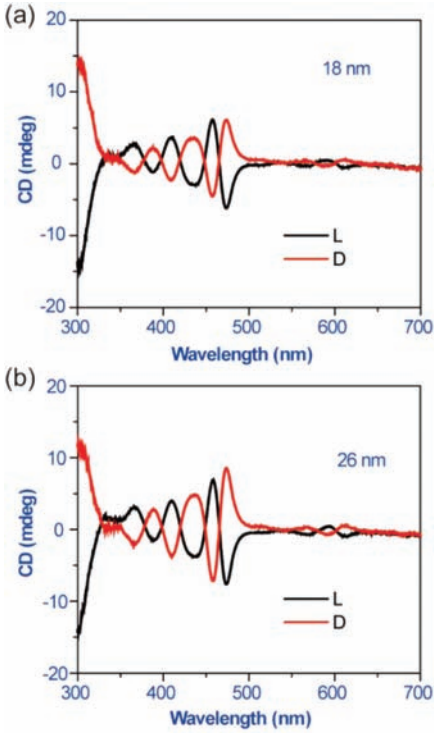


Fig. 2 (a and b) CD spectra of the 18 and 26 nm long CdSe/CdS dot/rod NCs.

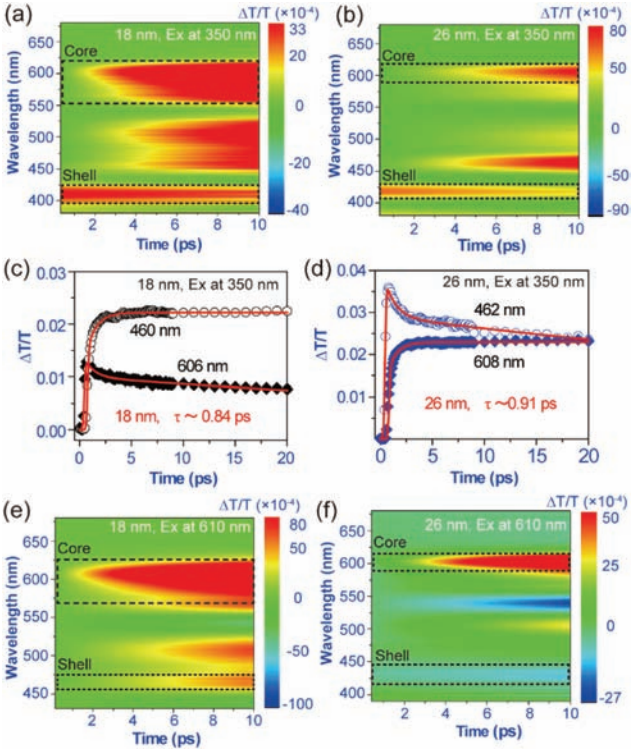


Fig. 3 (a and b) Time evolution of the fs-TA spectra at early time delays under 350 nm excitation for the 18 and 26 nm long NCs, respectively. (c and d) Normalized $\Delta T/T$ kinetics recorded at different probe wavelengths for the 18 and 26 nm long CdSe/CdS dot/rod NCs, respectively. (e and f) Time evolution of the fs-TA spectra at early times delays under 610 nm excitation for the 18 and 26 nm long NCs, respectively.

(Fig. 2). It can also be seen that their CD spectra have multiple peaks and valleys in the vicinity of the exciton absorption of the NCs. The anisotropic factors ($|g_{abs}|$) were determined to be $\sim 2.3 \times 10^{-4}$ for the 18 nm long NCs and $\sim 2.2 \times 10^{-4}$ for the 26 nm long NCs, according to the equation $g_{abs} = \Delta\varepsilon/\varepsilon = (A_L - A_R)/A$, where $A$ represents the conventional absorption of non-polarized light and $A_L$ and $A_R$ are the absorptions of left and right circularly polarized light, respectively.[22] Based on the theoretical calculation results of the D- and L-cysteine-stabilized $Cd_{10}Se_6S_{14}$ complexes, it was found that the wave function of the cysteine molecule can easily overlap with that of the CdSe/CdS NCs, so the induction of chirality was induced by the electronic state coupling between the L(D)-cysteine and the NCs. The surface distortion of the NCs caused by the cysteine molecule can be ruled out, due to no optical transition shift being observed in the D- and L-cysteine-stabilized CdSe/CdS NCs.[23] The efficient chirality of the CdSe/CdS NCs enables them to be promising materials for biological applications.

### Transient absorption spectra of the CdSe/CdS dot/rod NCs

To further reveal the photophysical properties of the CdSe/CdS dot/rod NCs, we investigated the ultrafast electron–hole dynamics of the CdSe/CdS dot/rod NCs by femtosecond transient absorption (fs-TA) spectroscopy.[24] Excitation at 350 and 610 nm was used to pump the CdS shell and CdSe core, respectively, of the 18 and 26 nm long NCs. In the case of 350 nm excitation, the e–h pairs were directly injected into the CdS electronic states. However, a large number of carriers could not be generated in the CdSe core due to its negligible light absorption. For both the 18 nm and 26 nm long NCs, the photoinduced absorption of the CdS shell at the blue edge builds up over a very short time frame (~0.3 ps) (Fig. 3a and b). For longer pump–probe delays, bleaching of the CdSe core appeared. Finally, the bleaching of CdSe becomes comparable to that of the CdS shell. The rate of bleaching formation for the CdS core (~0.84 and ~0.91 ps for the 18 and 26 nm long NCs) is well matched to the decay time of the CdSe shell, indicating that the electron wavefunction extends into the CdSe core after the injection of the e–h pairs into the CdSe core (Fig. 3c and d). Additionally, it was found that the geometric structure did not greatly influence the charge transfer dynamic processes in the CdSe/CdS dot/rod NCs. For 610 nm excitation, time traces of the CdSe core and the CdS shell are given in Fig. 3e and f. The e–h pairs were directly injected into the electronic states of both the CdSe core and the CdS shell. It was observed that their relevant ground state bleaching signals simultaneously appear within a very short time frame (~0.6 ps). It can be concluded that upon pumping the CdSe core, a ground-state bleaching signal can be induced in the CdS shell spectral region due to the delocalization of the electronic wavefunction. The ultrafast charge transfer between the CdSe core and the CdS shell can efficiently enhance the MPA of the CdSe/CdS dot/rod NCs, which will be discussed later.

### MPA properties of the CdSe/CdS dot/rod NCs

Two-photon absorption (2PA) cross-sections of the CdSe/CdS dot/rod NCs were then measured by using fs laser pulses from 720 to 880 nm (Fig. 4a). The 2PA mechanism can be confirmed by the measurements of the power-dependent PL intensity.[25] The quadratic dependence of their emission intensities on the input power confirms that the 2PA mechanism occurs at 800 nm (inset of Fig. 4a). The maximum 2PA cross-sections of the 18 and 26 nm long NCs were determined to be $3.5 \times 10^5$ and $6.2 \times 10^5$ GM at 800 nm, respectively. Compared to that of the 18 nm long NCs, the 2PA cross-section of the 26 nm long NCs was greatly enhanced by 1.8-fold, which was ascribed to the increased volume and stronger quantum confinement in the rod direction. As an important parameter, the 2PA action cross-sections ($\eta\delta$), which are the products of the QY and 2PA cross-section, were used to characterize the emission brightness of the two-photon contrast agents. The relevant values of the 18 and 26 nm long NCs were calculated to be $\sim 1.1 \times 10^4$ and $\sim 2.1 \times 10^4$ GM, respectively (Fig. 4b). Compared with other water-soluble semiconductor NCs and organic nanoparticles (Table 1),[11,26–29] our cysteine-capped CdSe/CdS dot/rod NCs exhibit comparable or much higher 2PA action cross-sections, indicating that they are promising materials for two-photon imaging applications.

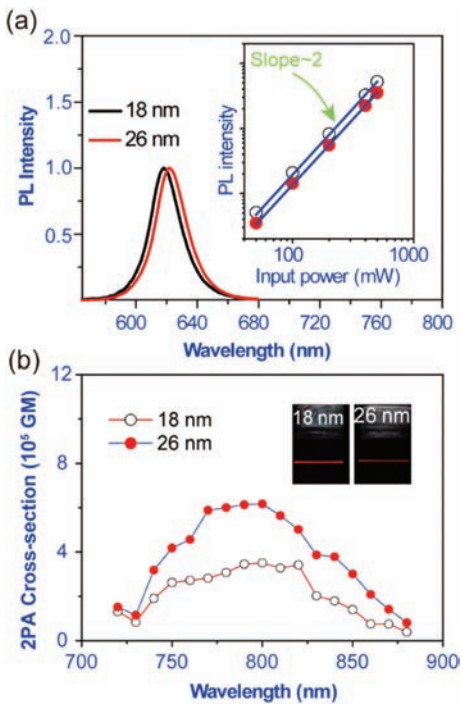


**Fig. 4** (a) Normalized PL spectra of the 18 and 26 nm long CdSe/CdS dot/rod NCs excited at 800 nm. The inset is the emission intensity as a function of the incident power for excitation at 800 nm shown with logarithmic scales. (b) The 2PA spectra of the 18 and 26 nm long NCs. The inset is the emission image excited at 800 nm.

Compared with two-photon excitation in the first biological window, *i.e.*, 700–900 nm, three-photon excitation in the second biological window, *i.e.*, 1000–1700 nm, has greater advantages, including a higher spatial resolution and an increased penetration depth.[30,31] Fig. 5a shows the emission intensity *versus* input power at 1300 nm. The slope of around 3 reveals that a 3PA process indeed occurs in both the 18 and 26 nm long NCs (inset of Fig. 5a). Their excitation wavelength-dependent 3PA cross-sections were then measured, with maximum values of $0.8 \times 10^{-76}$ and $1.4 \times 10^{-76}$ $cm^6$ $s^2$ per $photon^2$ at 1300 nm, respectively (Fig. 5b). Again, the maximum 3PA cross-section of the 26 nm long CdSe/CdS dot/rod NCs was much higher than that of the 18 nm long NCs. Additionally, the relevant 3PA action cross-sections were calculated to be $2.6 \times 10^{-78}$ and $4.6 \times 10^{-78}$ $cm^6$ $s^2$ per $photon^2$ for the 18 and 26 nm long NCs. To the best of our knowledge, these relevant values are among the largest measured for water-soluble semiconductor NCs and are larger by two orders of magnitude compared with those of organic nanoparticles (Table 1),[32,33] indicating the tremendous potential of these materials for deep-tissue bioimaging applications.

### Influence of the CdSe/CdS dot/rod NC chirality on cell cytotoxicity

Compared to that of carbon dots,[34] cytotoxicity is a major obstacle to the bioimaging application of semiconductor NCs and is mainly determined by two factors, *i.e.*, the core material of the NCs and their surface ligands.[35] For example, the cytotoxicity of CdSe/CdS dot/rod NCs was studied by Kirchner[36]

**Table 1** Calculated MPA action cross-sections of water-soluble cysteine-capped CdSe/CdS dot/rod NCs and previously reported water-soluble nanoparticles

| Sample | $\lambda_{em}$ (nm) | $\eta\sigma_2$ (GM) | $\eta\sigma_3$ ($cm^6$ $s^2$ per $photon^2$) | Ref. |
|---|---|---|---|---|
| CdS tetrapods | 500 | 3200 (130 fs, 650 nm) | N.A[a] | 11 |
| CdTe spherical NCs | 590 | <17 000 (130 fs, 803 nm) | N.A | 26 |
| Triphenylamine particles | 538 | 15 (150 fs, 827 nm) | N.A | 27 |
| CdTe/CdS spherical NCs | N.A | 1789 (340 fs, 515 nm) | N.A | 28 |
| CdSe/ZnS spherical NCs | 550 | 47 000 (700 nm, 100 fs) | N.A | 29 |
| Cyanostilbene particles | 516 | N.A | $1.9 \times 10^{-80}$ (1300 nm, 100 fs) | 32 |
| Diphenylamino particles | 642 | N.A | $1.68 \times 10^{-80}$ (1550 nm, 160 fs) | 33 |
| CdSe/CdS dot/rod NCs | 620 | 21 000 (800 nm, 100 fs) | $4.6 \times 10^{-78}$ (1300 nm, 100 fs) | This work |

[a] Not available.

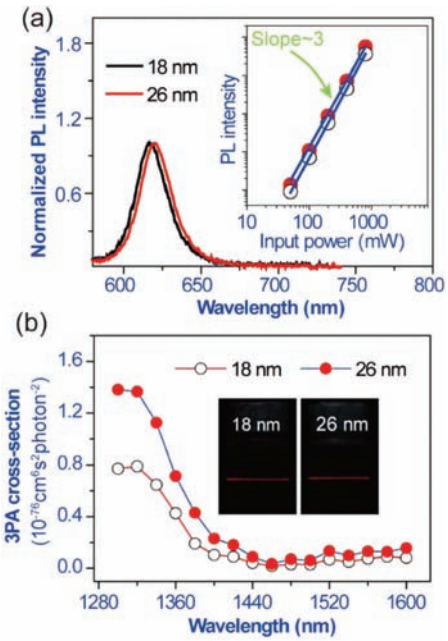


Fig. 5 (a) Normalized PL spectra of the 18 and 26 nm long CdSe/CdS dot/rod NCs excited at 1300 nm. The inset is the emission intensity as a function of the incident power for 1300 nm excitation, shown with logarithmic scales. (b) The 3PA spectra of the 18 and 26 nm long NCs. The inset is the emission image excited at 1300 nm.

and Pellegrino *et al.*,[37] respectively. It was found that the release of $Cd^{2+}$ ions from the core and surface chemistry are the major mechanisms of the observed cytotoxic effects of CdSe/CdS dot/rod NCs. There are three ways of reducing the NC toxicity: (1) using a low concentration of NCs, which requires them to have large MPA action cross-sections; (2) designing core–shell structured NCs, which can reduce the toxicity of the core; and (3) selecting appropriate capping ligands to reduce the NC toxicity.[38,39] Previous studies have indicated that chiral molecules on the surfaces of semiconductor NCs can significantly affect their toxicity, which may determine their ability to interact with biomolecules in the human body.[40] Therefore, the influence of the chirality on the cytotoxicity of NCs toward HeLa cells was determined. After incubating the cells with the 26 nm long D- or L-cysteine-stabilized CdSe/CdS dot/rod NCs at different concentrations for 24 h, their dark cytotoxicity was investigated (Fig. 6). Experimental results indicate that the cysteine-capped CdSe/CdS dot/rod NCs demonstrate good biocompatibility and can be used for cellular imaging. It can be concluded that the CdS shell and the cysteine ligand used for our CdSe/CdS dot/rod NCs are the main reasons for their low cytotoxicity. Additionally, it was found that the cell viability was chirality-independent, with the L-cysteine-stabilized CdSe/CdS dot/rod NCs being only slightly less-toxic compared with D-cysteine-stabilized NCs, probably due to the experimental error. In order to confirm that, we have incubated cells with the D- or L-cysteine at different concentrations for 24 h and investigated their dark cytotoxicity (Fig. S1†). It was found that the cytotoxicity of D- and L-cysteine

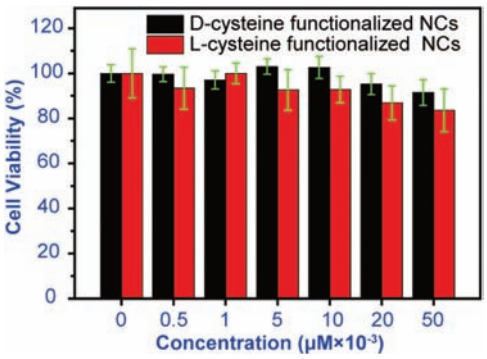


Fig. 6 Viabilities of HeLa cells treated with 26 nm long D- and L-cysteine-functionalized CdSe/CdS dot/rod NCs at different concentrations.

was at almost the same level, which was consistent with the relevant results obtained using D- and L-cysteine-stabilized CdSe/CdS dot/rod NCs. This chirality-independent cellular cytotoxicity indicates that there is no need for the selection of different stabilizer conformations during the design of bioimaging contrast agents. For the D- and L-cysteine-stabilized CdSe/CdS dot/rod NCs, the cell viability can be up to 90%, even at a high NC concentration of 5 nM. Additionally, due to the strong MPA action cross-sections of the NCs, very low concentrations can be used, which can further reduce the cytotoxicity of CdSe/CdS dot/rod NCs in biological applications.

### Two-photon FLIM

Due to the low dark cytotoxicity and high multiphoton PL brightness of the CdSe/CdS dot/rod NCs in the near-infrared region, they are promising materials for *in vivo* or *in vitro* imaging applications. The lifetime of the 26 nm long CdSe/CdS dot/rod NCs (11.4 ns) is long enough to eliminate autofluorescence (with a lifetime in the picosecond time scale[41]) or background signals in two-photon FLIM applications.[42,43] HeLa cells incubated with 26 nm long L-cysteine-stabilized dot/rod NCs (5 nM) were prepared for FLIM applications under 800 nm excitation. The intensity of two-photon FLIM reveals that the signals are evenly distributed across the cytoplasm (Fig. 7a), which was consistent with the results of two-photon

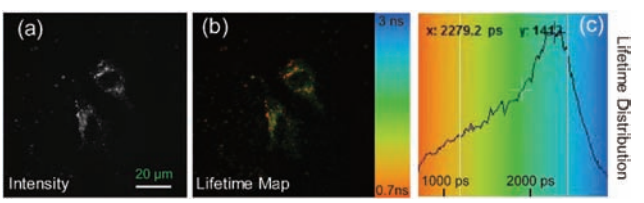


Fig. 7 Two-photon FLIM of HeLa cells incubated with 26 nm long L-cysteine-functionalized CdSe/CdS dot/rod NCs: fluorescence intensity (a), lifetime map (b) and lifetime distribution (c). The excitation wavelength is 800 nm, and the lifetime signals were recorded in the range of 550–650 nm.

confocal fluorescence imaging. Lifetime mapping reveals that the lifetime of the CdSe/CdS dot/rod NCs in the cellular environment is mainly distributed over a wide range from ~1500 to 2500 ps (Fig. 7b and c). More importantly, the short-lived autofluorescence signals were remarkably reduced. The experimental results presented here confirm that water-soluble cysteine-capped CdSe/CdS dot/rod NCs are promising materials for applications involving two-photon FLIM.

### Singlet oxygen generation

A large MPA and a high singlet oxygen generation efficiency ($\Phi_\Delta$) are required for the application of a photosensitizer in multiphoton-excited photodynamic therapy. It has been demonstrated that CdSe NCs are important photosensitizers because their triplet state is the lowest excited state and the relevant energy is greater than the energy of singlet oxygen (0.97 eV).[44,45] Due to the CdSe core of the water-soluble CdSe/CdS dot/rod NCs and their strong MPA, they may be an important family of multiphoton-excited photosensitizers. The characteristic emission peak of singlet oxygen at ~1270 nm (Fig. 8) unambiguously demonstrated that the water-soluble CdSe/CdS dot/rod NCs have the ability to generate singlet oxygen. Moreover, the 26 nm long CdSe/CdS dot/rod NCs exhibit stronger singlet oxygen generation than the 18 nm long NCs. Furthermore, using meso-5,10,15,20-tetrakis-(*N*-methyl-4-pyridyl)porphine as the standard, the $\Phi_\Delta$ efficiencies of the 18 and 26 nm long CdSe/CdS dot/rod NCs were determined to be 25% and 35%, respectively. Compared to those of the bare CdSe spherical NCs (~5% in toluene), the great improvement in the $\Phi_\Delta$ efficiencies of the CdSe/CdS dot/rod NCs should be induced by the defect passivation effect of the CdS shell and surface cysteine ligands, as well as the light-harvesting effect of the CdS shell. The product of MPA cross-sections and $\Phi_\Delta$ values of NCs, which can be used to characterize their multiphoton-excited singlet oxygen generation capability, will also be very large, *i.e.*, $8.8 \times 10^4$ ($2.0 \times 10^{-77}$) and $2.2 \times 10^5$ GM

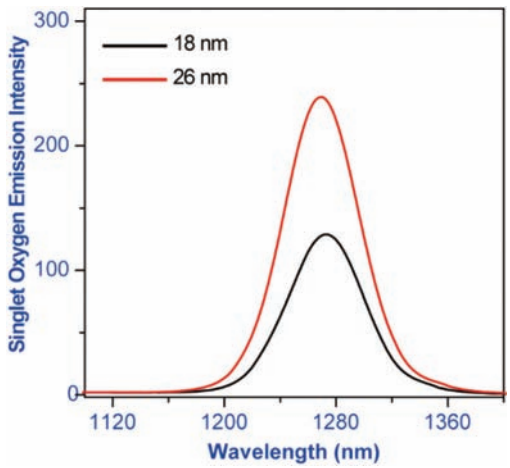


Fig. 8 Characteristic singlet oxygen emission at ~1270 nm generated by the 18 and 26 nm long CdSe/CdS dot/rod NCs in $CD_3OD$ under 350 nm excitation.

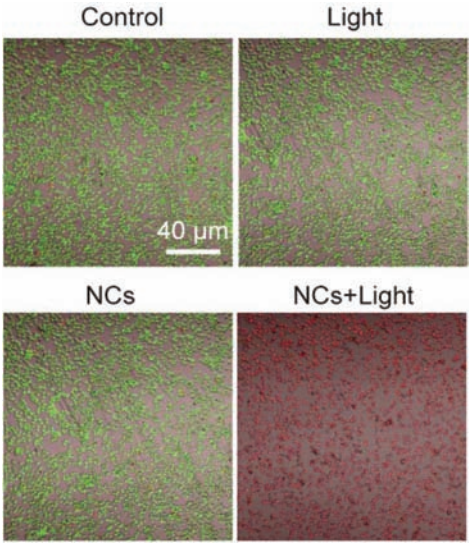


Fig. 9 Cancer cell viability after treatment with L-cysteine-functionalized CdSe/CdS dot/rod NCs (5 nM) with or without two-photon irradiation at 800 nm. Live cells were distinguished by calcein AM, which has a green color, and dead cells were distinguished by PI, which has a red color.

($4.9 \times 10^{-77}$ $cm^6$ $s^2$ per $photon^2$) for the 18 and 26 nm long CdSe/CdS dot/rod NCs, respectively, under two- (three-) photon excitation. These results indicate that water-soluble cysteine-capped CdSe/CdS dot/rod NCs can be utilized as multiphoton excited photosensitizers.

### Two-photon excited PDT

Considering the high $\Phi_\Delta$ efficiencies of the NCs, their two-photon excited PDT capacity in cells was further verified (Fig. 9). In the experiments, calcein AM, which has a green color, and propidium iodide (PI), which has a red color, cellular viability kits were used to distinguish between living cells and dead cells, respectively. HeLa cells showed good viability under only two-photon irradiation or without the NCs, indicating that the HeLa cells had strong resistance to two-photon irradiation and low dark cytotoxicity. In sharp contrast, under the combined action of two-photon irradiation and the NCs, cell contraction and the formation of a large number of bubbles were observed, accompanied by an enhancement of the red fluorescence, which proved the excellent two-photon excited PDT effect of the CdSe/CdS dot/rod NCs. The above experimental results suggested that two-photon irradiation on the NC-incubated HeLa cells could accelerate the death of cancer cells, directly confirming the dominant role of reactive oxygen species (ROS, *e.g.*, $^1O_2$) in PDT.

## Conclusions

In summary, we have developed water-soluble cysteine-capped CdSe/CdS dot/rod NCs with different aspect ratios. The NCs exhibit long lifetime, efficient CD and ultrafast

carrier relaxation dynamics. More importantly, the CdSe/CdS dot/rod NCs exhibit large MPA action cross-sections in the first and second biological windows, $2.1 \times 10^4$ GM at 800 nm and $4.6 \times 10^{-78}$ $cm^6$ $s^2$ per $photon^2$ at 1300 nm, which are sufficiently high for biological applications, including two-photon FLIM. Moreover, the CdSe/CdS dot/rod NCs exhibit high singlet oxygen generation activity, indicating that they are promising multiphoton-excited PDT agents. These results suggest that water-soluble cysteine-capped CdSe/CdS dot/rod NCs can be developed as promising novel contrast agents for biological applications.

# Experimental

### Sample preparation

The detailed synthetic procedures for the CdSe/CdS dot/rod NCs were slightly modified from the procedures described in our previous work.[23]

### Characterization

The measurements of the linear absorption spectra were carried out using a UV–Vis–NIR spectrophotometer (Lambda 950, PerkinElmer, Inc.), while the one-photon excited PL spectra were recorded with a PL spectrometer (Zolix, SENS-9000). The morphology and size of the CdSe/CdS dot/rod NCs were investigated by TEM (JEOL, JEM-2010). The fluorescence lifetimes were measured using a compact fluorescence lifetime spectrometer (Hamamatsu, model C11367). CD spectra were recorded using a Jasco 1500 spectrometer. The singlet oxygen emission spectra were measured by using a Fluorolog-3 iHR spectrofluorometer (Jobin–Yvon) equipped with a near-infrared sensitive photomultiplier tube (Hamamatsu, model R5509-72) operated at −80 °C. An 850 nm long-pass filter was placed before the detector.

### Measurement of the fs-TA spectra

The measurements were performed using a pump–probe setup (18SI80466 Rev.1, Newport). The samples were pumped with excitation pulses (100 fs, 1000 Hz) at 350 or 610 nm, which were generated using a fs mode-locked Ti-sapphire laser (Spectra Physics). The samples were probed with a white-light continuum (350–750 nm) that was generated by focusing a small portion of the fundamental 800 nm laser pulses into a thin $CaF_2$ plate. The probe beam was then delayed with respect to the pump beam by a mechanical delay stage with a resolution of 50 fs. The transmitted probe light was then dispersed and detected using a spectrometer.

### Measurements of the multiphoton-excited PL spectra

During the measurements, the laser beam was focused onto a quartz cell filled with the CdSe/CdS dot/rod NCs solution, and the multiphoton-excited PL spectra were recorded using a compact spectrometer, with a direction perpendicular to the pump beam.

### Determination of the MPA cross-sections

The MPA coefficients of the CdSe/CdS dot/rod NCs were determined by open aperture *Z*-scan measurements.[46] After obtaining the 2PA coefficient ($\beta$, in units of cm $W^{-1}$), the values of $\sigma_2$ (in units of $cm^2$ s per photon) can be deduced from the following equation:

$$\beta = \frac{\sigma_2 N_A d \times 10^{-3}}{h\nu} \quad (1)$$

where $N_A$ is the Avogadro constant, $d$ is the concentration, $h$ is the Planck constant, and $\nu$ is the frequency of the incident beam.[47] Correspondingly, the values of $\sigma_3$ (in units of $cm^4$ $s^2$ per $photon^2$) can be deduced from the following equation:

$$\gamma = \frac{\sigma_3 N_A d \times 10^{-3}}{(h\nu)^2} \quad (2)$$

where $\gamma$ is the 3PA coefficient of the CdSe/CdS dot/rod NCs in units of $cm^3$ $W^{-2}$.[48]

### Experimental details of two-photon FLIM, measurements of the singlet oxygen generation efficiency and two-photon PDT

The relevant experimental details are described in the ESI.†

# Conflicts of interest

There are no conflicts to declare.

# Acknowledgements

This work is supported by the Shenzhen Science and Technology Innovation Commission (Projects No: JCYJ20170302142433007, KQJSCX20170726145748464 and JCYJ20180305180553701), the National Natural Science Foundation of China (No. 61805118, 11574130 and 61875082), the Synergetic Innovation Center for Organic Electronics and Information Displays, the Natural Science Foundation of Jiangsu Province of China (No. BK20171020), the China Postdoctoral Science Foundation (No. 2017M621733 and 2018T110488), the Materials Characterization and Preparation Center of Southern University of Science and Technology and the open research fund of the Key Laboratory for Organic Electronics and Information Displays.

# Notes and references

1 P. Reiss, M. Protière and L. Li, *Small*, 2009, **5**, 154–168.
2 N. S. Makarov, P. C. Lau, C. Olson, K. A. Velizhanin, K. M. Solntsev, K. Kieu, S. Kilina, S. Tretiak, R. A. Norwood, N. Peyghambarian and J. W. Perry, *ACS Nano*, 2014, **8**, 12572–12586.
3 T. He, J. Li, X. Qiu, S. Xiao, C. Yin and X. Lin, *Adv. Opt. Mater.*, 2018, **6**, 1800843.

4 G. Xing, S. Chakrabortty, K. L. Chou, N. Mishra, C. H. A. Huan, Y. Chan and T. C. Sum, *Appl. Phys. Lett.*, 2010, **97**, 061112.
5 C. Zhang, F. Zhang, S. Qian, N. Kumar, J. Hahm and J. Xu, *Appl. Phys. Lett.*, 2008, **92**, 233116.
6 R. Subha, V. Nalla, E. J. Q. Lim, C. Vijayan, B. B. S. Huang, W. S. Chin and W. Ji, *ACS Photonics*, 2015, **2**, 43–52.
7 G. Xing, S. Chakrabortty, S. W. Ngiam, Y. Chan and T. C. Sum, *J. Phys. Chem. C*, 2011, **115**, 17711–17716.
8 L. Jing, S. V. Kershaw, Y. Li, X. Huang, Y. Li, A. L. Rogach and M. Gao, *Chem. Rev.*, 2016, **116**, 10623–10730.
9 J. Zhou, Y. Yang and C. Zhang, *Chem. Rev.*, 2015, **115**, 11669–11717.
10 D. R. Larson, W. R. Zipfel, R. M. Williams, S. W. Clark, M. P. Bruchez and F. W. Wise, *Science*, 2003, **300**, 1434.
11 D. Wawrzyńczyk, *J. Mater. Chem. C*, 2017, **5**, 1724–1729.
12 S. Selvan, T. Tan and J. Ying, *Adv. Mater.*, 2005, **17**, 1620–1625.
13 F. D. Stasio, J. Q. Grim, V. Lesnyak, P. Rastogi, L. Manna, I. Moreels and R. Krahne, *Small*, 2015, **11**, 1328–1334.
14 T. He, J. Li, X. Li, C. Ren, Y. Luo, F. Zhao, R. Chen, X. Lin and J. Zhang, *Appl. Phys. Lett.*, 2017, **111**, 151102.
15 Y. Li, J. Cheng, J. Li, X. Zhu, T. He, R. Chen and Z. Tang, *Angew. Chem., Int. Ed.*, 2018, **57**, 10236.
16 Y. Zhou, M. Yang, K. Sun, Z. Tang and N. A. Kotov, *J. Am. Chem. Soc.*, 2010, **132**, 6006–6013.
17 M. Shahrajabian, F. Ghasemi and M. R. Hormozi-Nezhad, *Sci. Rep.*, 2018, **8**, 14011.
18 L. Carbone, C. Nobile, M. D. Giorgi, F. D. Sala, G. Morello, P. Pompa, M. Hytch, E. Snoeck, A. FioreIsabella, R. Franchini, M. Nadasan, A. F. Silvestre, L. Chiodo, S. Kudera, R. Cingolani, R. Krahne and L. Manna, *Nano Lett.*, 2007, **7**, 2942–2950.
19 D. V. Talapin, J. H. Nelson, E. V. Shevchenko, S. Aloni, B. Sadtler and A. P. Alivisatos, *Nano Lett.*, 2007, **7**, 2951–2959.
20 M. Zavelani-Rossi, R. Krahne, G. Della Valle, S. Longhi, I. R. Franchini, S. Girardo, F. Scotognella, D. Pisignano, L. Manna, G. Lanzani and F. Tassone, *Laser Photonics Rev.*, 2012, **6**, 678–683.
21 M. Zavelani-Rossi, M. G. Lupo, R. Krahne, L. Manna and G. Lanzania, *Nanoscale*, 2010, **2**, 931–935.
22 J. E. Field, G. Muller, J. P. Riehl and D. Venkataraman, *J. Am. Chem. Soc.*, 2003, **125**, 11808–11809.
23 J. Cheng, J. Hao, H. Liu, J. Li, J. Li, X. Zhu, X. Lin, K. Wang and T. He, *ACS Nano*, 2018, **12**, 5341–5350.
24 M. Grazia Lupo, F. D. Sala, L. Carbone, M. Zavelani-Rossi, A. Fiore, L. Lüer, D. Polli, R. Cingolani, L. Manna and G. Lanzani, *Nano Lett.*, 2008, **8**, 4582–4587.
25 G. S. He, L. Tan, Q. Zheng and P. N. Prasad, *Chem. Rev.*, 2008, **108**, 1245–1330.
26 L. Pan, N. Tamai, K. Kamada and S. Deki, *Appl. Phys. Lett.*, 2007, **91**, 051902.
27 V. Parthasarathy, S. Fery-Forgues, E. Campioli, G. Recher, F. Terenziani and M. Blanchard-Desce, *Small*, 2011, **7**, 3219–3229.
28 J. Li, S. Zhang, H. Dong, Y. Ma, B. Xu, J. Wang, Z. Cai, Z. Chen and L. Zhang, *Part. Part. Syst. Charact.*, 2017, **34**, 1600193.
29 D. R. Larson, W. R. Zipfel, R. M. Williams, S. W. Clark, M. P. Bruchez, F. W. Wise and W. W. Webb, *Science*, 2003, **300**, 1434.
30 Kenry, Y. Duan and B. Liu, *Adv. Mater.*, 2018, **30**, 1802394.
31 C. Ren, X. Deng, W. Hu, J. Li, X. Miao, S. Xiao, H. Liu, Q. Fan, K. Wang and T. He, *Chem. Commun.*, 2019, **55**, 5111–5114.
32 A. K. Mandal, S. Sreejith, T. He, S. K. Maji, X. Wang, S. L. Ong, J. Joseph, H. Sun and Y. Zhao, *ACS Nano*, 2015, **9**, 4796–4805.
33 Y. Wang, M. Chen, N. Alifu, S. Li, W. Qin, A. Qin, B. Z. Tang and J. Qian, *ACS Nano*, 2017, **11**, 10452–10461.
34 L. Xiao and H. Sun, *Nanoscale Horiz.*, 2018, **3**, 565–597.
35 J. Zhou, Y. Yang and C. Zhang, *Chem. Rev.*, 2015, **115**, 11669–11717.
36 C. Kirchner, T. Liedl, S. Kudera, T. Pellegrino, A. M. Javier, H. E. Gaub, S. Stölzle, N. Fertig and W. J. Parak, *Nano Lett.*, 2005, **5**, 331–338.
37 T. Pellegrino, L. Manna, S. Kudera, T. Liedl, D. Koktysh, A. L. Rogach, S. Keller, J. Rädler, G. Natile and W. J. Parak, *Nano Lett.*, 2004, **4**, 703–707.
38 A. Hoshino, K. Fujioka, T. Oku, M. Suga, Y. F. Sasaki, T. Ohta, M. Yasuhara, K. Suzuki and K. Yamamoto, *Nano Lett.*, 2004, **4**, 2163.
39 N. Chen, Y. He, Y. Su, X. Li, Q. Huang, H. Wang, X. Zhang, R. Tai and C. Fan, *Biomaterials*, 2012, **33**, 1238–1244.
40 Y. Li, Y. Zhou, H. Wang, S. Perrett, Y. Zhao, Z. Tang and G. Nie, *Angew. Chem., Int. Ed.*, 2011, **50**, 5860–5864.
41 M. Y. Berezin and S. Achilefu, *Chem. Rev.*, 2010, **110**, 2641–2684.
42 W. Hu, Q. Wang, X. Miao, L. Bai, L. Li, G. S. He, J. Li, S. Yao, T. He, X. Lu, W. Huang, P. N. Prasad and Q. Fan, *J. Phys. Chem. C*, 2018, **122**, 20945–20951.
43 T. He, C. Ren, Z. Li, S. Xiao, J. Li, X. Lin, C. Ye, J. Zhang, L. Guo, W. Hu and R. Chen, *Appl. Phys. Lett.*, 2018, **112**, 211102.
44 A. C. S. Samia, X. Chen and C. Burda, *J. Am. Chem. Soc.*, 2003, **125**, 15736–15737.
45 R. Bakalova, H. Ohba, Z. Zhelev, M. Ishikawa and Y. Baba, *Nat. Biotechnol.*, 2004, **22**, 1360–1361.
46 M. Sheik-Bahae, A. A. Said, T.-H. Wei, D. J. Hagan and E. W. Van Stryland, *IEEE J. Quantum Electron.*, 1990, **26**, 760–769.
47 G. S. He, G. C. Xu, P. N. Prasad, B. A. Reinhardt, J. C. Bhatt and A. G. Dillard, *Opt. Lett.*, 1995, **20**, 435–437.
48 G. S. He, J. D. Bhawalkar, P. N. Prasad and B. A. Reinhardt, *Opt. Lett.*, 1995, **20**, 1524–1526.